Coupled Shell Model of Turbulence

Alfred B. Hansen

January 29, 2024

Abstract

Shell models of turbulence reproduce some of the few known results about turbulence. These models are reduced wavenumber models, more suitable for simulations rather than direct numerical simulations of the Navier-Stokes equation. In this project, we couple two such models, with the intent of replicating the inherent 3D and 2D scaling behaviour of atmospheric turbulence. The coupled model, based on the so-called Sabra model, shows different scaling properties depending on parameter choices, but the 3D regime dominates, likely due to an asymmetry of energy cascades in the Sabra model.

Contents

1 Introduction

Large scale simulations of fluid flow using Navier-Stokes equation (NSE) is computationally costly, and at large Reynolds numbers (Re) infeasible. One course of action is therefore to construct simpler models that capture the qualitative behaviour of the NSE. The aptly named shell models, which are reduced wavenumber models of turbulence, accomplish this by mimicking the triad interactions seen in the spectral form of the NSE in a reduced model with next-nearest neighbour interactions between shells.

The large scale motion of the atmosphere can be seen as a barotropic fluid, and therefore arguably well-described as 2D, however on smaller spatial scales 3D [4]. One would therefore expect the scaling of the spectrum to look like 2D turbulence at large scales (small wave numbers), and 3D at small scales (large wave numbers), which is indeed the case [5].

The *Sabra* shell model, models either 2D or 3D turbulence depending on the choice of the parameter ϵ, capturing the scaling relations of the celebrated K41 scaling theory of turbulence, but can therefore not by itself be expected to capture both the 2D and 3D regimes of atmospheric turbulence. The goal of this project is therefore to couple two Sabra models, one 3D and another 2D, with next-nearest neighbour interactions also between the two models, to investigate whether such a model can display 2D and 3D scaling at respectively small and large wave numbers.

2 Sabra model

We start by giving a brief overview of the Sabra shell model, following that of [2]. The Sabra model [1] is a reduced wavenumber model, based on the spectral NSE. Assuming incompressibility, the NSE can, using Einstein summation notation, be written as

$$\partial_t u_i + u_j \partial_j u_i = -\partial_i p + Re^{-1} \partial_{jj} u_i + f_i \tag{1}$$

where p is the pressure field, f_i the external forces, and u_i the i'th component of the velocity field $\vec{u}(\boldsymbol{x}, t)$. Together with the continuity equation

$$\partial_i u_i = 0 \tag{2}$$

it describes the flow of an incompressible fluid. For large Reynolds numbers the flow becomes turbulent, as it is dominated by the nonlinear terms. One can write the NSE on spectral form, by introducing a spectral velocity

$$u_i(\boldsymbol{k}) = \frac{1}{(2\pi)^3} \int e^{-i\boldsymbol{k}\boldsymbol{x}} u_i(\boldsymbol{x}) d\boldsymbol{x} \tag{3}$$

such that the spectral NSE, after discretising the Fourier space by assuming a finite box with sides L and periodic boundary conditions, takes the form

$$\partial_t u_i(\boldsymbol{k}) = -ik_j \sum_{\boldsymbol{k'}} \left(\delta_{il} - \frac{k_i k'_l}{k^2} \right) u_j(\boldsymbol{k'}) u_l(\boldsymbol{k} - \boldsymbol{k'}) - \frac{\nu L}{2\pi} k^2 u_i(\boldsymbol{k}) + f_i(\boldsymbol{k}) \tag{4}$$

We note one of many interesting results of eq. (4), by writing the rate of change of the energy $E = \frac{1}{2} \sum_i u_i^2(\boldsymbol{k})$ in the unforced and inviscid case ($f_i = \nu = 0$), nothing that $u_i(\boldsymbol{k}) \in \mathbb{C}$ so $u_i^2(\boldsymbol{k}) = u_i^*(\boldsymbol{k}) u_i(\boldsymbol{k})$, as

$$\dot{E} = \frac{1}{2} \sum_i u_i^*(\boldsymbol{k}) \partial_t u_i(\boldsymbol{k}) + c.c \tag{5}$$

$$= \frac{-ik_j}{2} \sum_i \sum_{\boldsymbol{k'}} \left(\delta_{il} - \frac{k_i k'_l}{k^2} \right) u_i^*(\boldsymbol{k}) u_j(\boldsymbol{k'}) u_l(\boldsymbol{k} - \boldsymbol{k'}) + c.c \tag{6}$$

Using that $u_i(\boldsymbol{x})$ is real, such that $u_i^*(\boldsymbol{x}) = u_i(\boldsymbol{x})$ we see that

$$u_i^*(\boldsymbol{k}) = \frac{1}{(2\pi)^3} \int e^{i\boldsymbol{k}\boldsymbol{x}} u_i^*(\boldsymbol{x}) d\boldsymbol{x} = \frac{1}{(2\pi)^3} \int e^{-(-i\boldsymbol{k}\boldsymbol{x})} u_i(\boldsymbol{x}) d\boldsymbol{x} = u_i(-\boldsymbol{k}) \tag{7}$$

And now $\dot{E}$ can be written as

$$\dot{E} = \frac{ik_j}{2} \sum_i \sum_{\boldsymbol{k'}} \left(\delta_{il} - \frac{k_i k'_l}{k^2} \right) u_i(-\boldsymbol{k}) u_j(\boldsymbol{k'}) u_l(\boldsymbol{k} - \boldsymbol{k'}) \tag{8}$$

showing that the change in energy only happens through triads of spectral velocities with wavenumbers adding to 0, since $-\boldsymbol{k} + \boldsymbol{k'} + (\boldsymbol{k} - \boldsymbol{k'}) = 0$, where we can simply relabel $\boldsymbol{k} - \boldsymbol{k'} = \boldsymbol{k''}$.

Equation (4) is the usual starting point for shell models. In shell models, the number of wavenumbers $\boldsymbol{k}$ is reduced, by dividing Fourier-space into concentric spheres with some spacing λ and truncating the range of wavenumbers, by choosing a number of shells N and writing the n'th wavenumber as $k_n = k_0 \lambda^n$. Here k_n only represents the radius of the n'th concentric sphere and the wavenumber is therefore effectively 1-dimensional, instead of a 3-dimensional vector. This is reasonable if one assumes the fluid to be isotropic and homogeneous, such that there is no preferred direction. Greatly reducing Fourier-space makes the shell models unphysical, in the sense that one cannot simply transform the spectral velocities simulated by shell models to real space to obtain a velocity field.

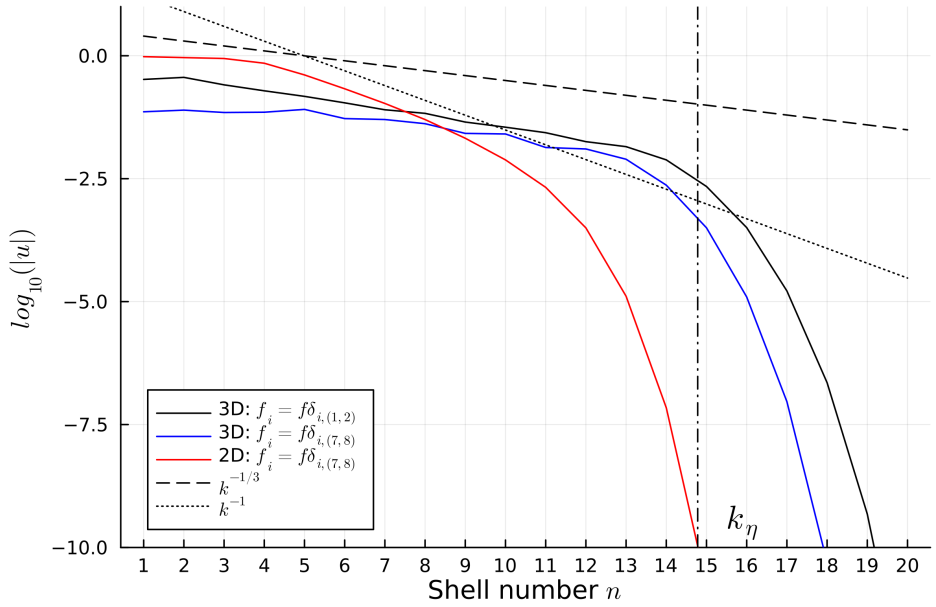

Figure 1: Velocity spectra from simulations of the Sabra model in the 3D ($\epsilon = 1/2$) and 2D ($\epsilon = 5/4$) regimes, with forcing indicated with the notation $f_i = f\delta_{i,(A,B)}$, which is shorthand for $f \times (\delta_{i,A} + \delta_{i,B})$. Parameters used are $[f,\, \lambda,\, k_0,\, N,\, \nu,\, \Delta t] = \left[0.1 \times (1+i),\, 2,\, 1,\, 20,\, 5 \times 10^{-7},\, 5 \times 10^{-5}\right]$, and all 3 setups have been integrated for a total time $t = 200$. The estimated Kolmogorov scale is indicated by the k_η line (dash-dot), together with k^{-1} and $k^{-1/3}$ (dashed and dotted lines).

The Sabra model has the governing equation

$$\dot{u}_n = ik_n \left(u^*_{n+1} u_{n+2} - \frac{\epsilon}{\lambda} u^*_{n-1} u_{n+1} - \frac{\epsilon - 1}{\lambda} u_{n-2} u_{n-1} \right) - \nu k_n^2 u_n + f_n \tag{9}$$

where $\{u_n\} \in \mathbb{C}$ are the spectral velocities associated with shell n, f_n the external forcing on the n'th shell, ν the viscosity and the parameter ϵ determines whether the model displays 3D or 2D turbulence. This can be seen by looking at the inviscid invariants, which are the conserved sums in the case of no forcing and dissipation. The first inviscid invariant is the energy

$$E^{(1)} = \sum_{n=1}^{N} |u_n|^2 \tag{10}$$

and the second inviscid invariant is

$$E^{(2)} = \sum_{n=1}^{N} \left(\frac{1}{\epsilon - 1} \right)^n |u_n|^2 \tag{11}$$

which, depending on ϵ, is interpreted as either the generalised enstrophy ($\epsilon > 1$), corresponding to the model displaying 2D turbulence, or helicity ($\epsilon < 1$) which can be both positive and negative corresponding to 3D turbulence. The nonlinear interaction in the Sabra model is restricted to the next-nearest neighbours, reducing the number of triads contributing to the rate of change of the energy to 3, and the relative strength of the nonlinear interactions are determined by ϵ.

Kolmogorov's 1941 theory [3] tells us, by use of simple dimensional analysis, that the spectral velocities for 3D turbulence should scale as $|u| \sim k^{-1/3}$. In Figure 1 the Sabra model has been simulated for 3D ($\epsilon = 1/2$) and 2D ($\epsilon = 5/4$) where the Kolmogorov scaling is clearly seen for the 3D cases.

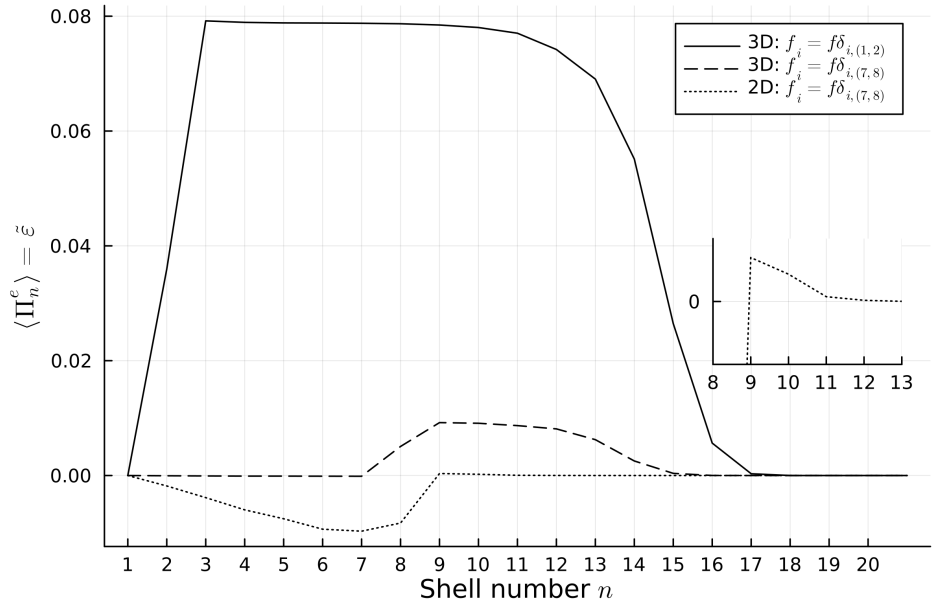

Figure 2: Energy fluxes $\langle \Pi_n^e \rangle$ for 3 different realisations of the Sabra model, with parameters corresponding to that of Figure 1. In both 3D cases the transport of energy from small to large wavenumbers is evident, while the opposite is true for 2D. **Inset**: Zoom in on the flux of the 2D Sabra model, where a small positive flux for wavenumers larger than the forcing shell numbers 7 and 8 is seen.

In Figure 1 we have indicated the Kolmogorov scale η for the 3D model with forcing $f_n = (1 + i)(\delta_{n,1} + \delta_{n,2})$, after which the dissipative effects (loss of eddies to heat the system) become significant, and the Kolmogorov scaling no longer holds. The scale η has been estimated by finding the mean energy flux as

$$\langle \Pi_n^e \rangle = \langle \Delta_{n+1} - (\epsilon - 1)\Delta_n \rangle \tag{12}$$

$$= k_n \left\langle \Im \left(u_n^* u_{n+1}^* u_{n+2} - \frac{\epsilon - 1}{\lambda} u_{n-1}^* u_n^* u_{n+1} \right) \right\rangle \tag{13}$$

where we have used the correlators $\Delta_n = k_{n-1}\Im(u_{n-1}^* u_n^* u_{n+1})$. The energy flux is shown in Figure 2 and the mean dissipation due to non-linear terms $\tilde{\varepsilon}$ is estimated as the mean energy flux in the range where it is approximately constant. The relation

$$\eta \sim \left(\frac{\tilde{\varepsilon}}{\nu^3} \right)^{-1/4} \tag{14}$$

estimates η and thus the wavenumber at which the dissipation becomes significant is $k_\eta \sim \eta^{-1}$. In Figure 2 we clearly see that the flux of energy in the 3D cases are towards larger wavenumbers and for the 2D case a flux of energy towards small wavenumbers, but a sligt flux towards larger wave numbers. In the Sabra model we thus have a cascade of energy in towards large k for 3D and in 2D a transport of energy mainly towards small k and enstrophy towards large k, as seen in Figure 3, where the enstrophy flux

$$\langle \Pi_n^z \rangle = \left\langle \left(\frac{1}{\epsilon - 1} \right)^n (\Delta_{n+1} - \Delta_n) \right\rangle \tag{15}$$

$$= k_n \left\langle \left(\frac{1}{\epsilon - 1} \right)^n \Im \left(u_n^* u_{n+1}^* u_{n+2} - \frac{1}{\lambda} u_{n-1}^* u_n^* u_{n+1} \right) \right\rangle \tag{16}$$

has been plotted for the 2D Sabra model. This indicates that he slope of $log(|u|)$ should more so follow the energy scaling $k^{-1/3}$ before the shells numbers where forcing is applied, and the enstrophy scaling k^{-1} after, which is seen in Figure 1. The missing inverse cascade of energy in the 2D Sabra model is an asymmetry of note, as this will probably affect a model of coupled 2D and 3D Sabra models.

The scaling behaviour in Figure 1 can be seen by looking at some inviscid function $I = 1/2 \sum_{n=1}^{N} k_n^\alpha |u|^2$, and the flux at some shell n', which should equal the dissipation of the function $\tilde{\varepsilon}_I$, such that

$$\begin{aligned} \tilde{\varepsilon}_I = \dot{I}|_{n \leq n'} &= \sum_{n=1}^{n'} k_n^\alpha u_n \partial_t u_n \\ &= i \sum_{n=1}^{n'} k_n^{\alpha+1} u_n \left(u_{n+1}^* u_{n+2} - \frac{\epsilon}{\lambda} u_{n-1}^* u_{n+1} - \frac{\epsilon - 1}{\lambda} u_{n-2} u_{n-1} \right) \end{aligned} \tag{17}$$

and thus the scaling $\tilde{\varepsilon}_I \sim k_n^{\alpha+1} u_n^3$ from which it follows that $u_n \sim k_n^{-\frac{\alpha+1}{3}}$, where $\alpha = \Re\left(\frac{log(|1/(\epsilon-1)|) + i\pi}{log(\lambda)} \right)$ is 0 for the energy and 2 for $\lambda = 2$ and $\epsilon = 5/4$.

3 Coupled Model

To obtain a shell model that captures the inherently 3D and 2D effects of the atmosphere at different scales, we couple two Sabra models with different ϵ-values, allowing for nearest and next-nearest neighbour interactions in triads, also between the tow Sabra models. We assume that both models have N shells and the same shell spacing such that $k_n = k_0 \lambda^n$,

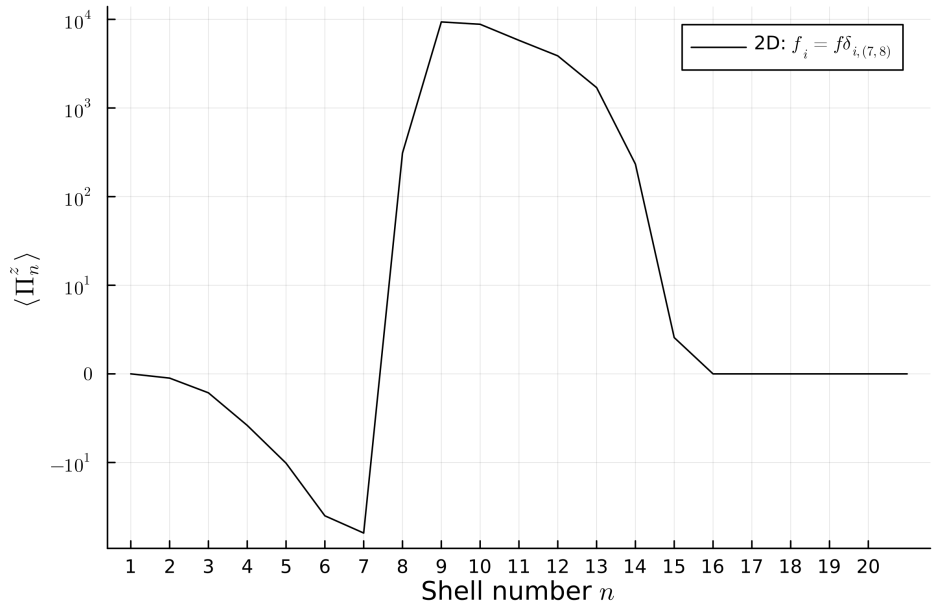

Figure 3: Enstrophy flux $\langle \Pi_n^z \rangle$ for the 2D sabra model, with parameters as in Figure 1. The enstrophy is clearly transported towards larger wavenumbers, however some enstrophy is also transported to smaller.

where $n = 1, 2...N$. The n'th spectral velocity are denoted $u_n^{(i)}$, where $i = 1, 2$ indicates if it is a shell in the first or second model, which we will also call chain interchangeable in the following. To obtain the model, we assume that the nonlinear terms are a combination of all possible triad interactions. The conservation of helicity/enstrophy is trivially broken, however since both chains conserve energy we expect this to hold true also for the coupled model.

Starting from the governing equations $\dot{u}_n^{(1)}$ and $\dot{u}_n^{(2)}$ with no dispersion or forcing, where the non-linear terms are the possible next-nearest neighbour terms, we search for conserved integrals of the form

$$E^\alpha = \sum_n k_n^\alpha \left(\left| u_n^{(1)} \right|^2 + \left| u_n^{(2)} \right|^2 \right) \tag{18}$$

For these to be conserved demands that

$$\dot{E}^\alpha = \sum_n k_n^\alpha \left(u_n^{*(1)} \dot{u}_n^{(1)} + u_n^{*(2)} \dot{u}_n^{(2)} + c.c. \right) = 0 \tag{19}$$

The triad interactions can be ordered by their diagrams, and reordered such that they are translations in shell number of each other, taking on the typical form $(ak_n + bk_{n+1} + ck_{n+1})u_n^{(i)} u_{n+1}^{(j)} u_{n+2}^{(k)}$ as in [2], and thus $\dot{E}^\alpha$ can be written as sum of translated diagrams[1]. Demanding that $ak_n + bk_{n+1} + ck_{n+1} = 0$ then fixes the model parameters. We showcase an example of all triads of the form $u_{n-1}^i u_n^j u_{n+1}^i$, which we will denote $\wedge$'s or $\vee$'s, drawn in Figure 4. The rate of change in E^α due to the triads in these diagrams are denoted $\dot{E}^\alpha_{\wedge\vee}$ and can be written as

[1]One exception is the special case of diagrams containing terms like $u_n^{(i)} u_n^{(j)}$, see *Appendix A*.

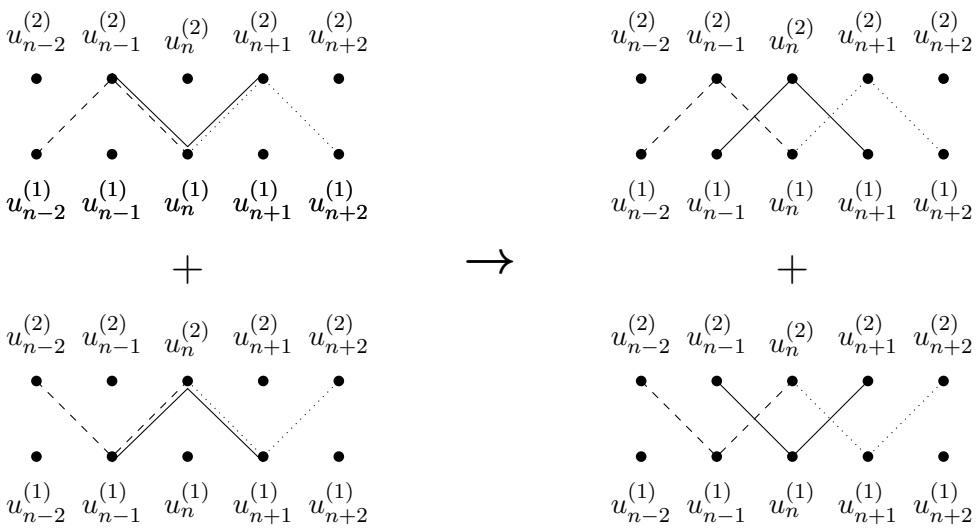

Figure 4: **Left**: Diagrams of the possible triad interactions with the form $u^i_n u^j_{n+1} u^i_{n+2}$, which are the diagrams associated with $\dot{u}^{(1)}_n$ (top) and $\dot{u}^{(2)}_n$ (bottom). **Right**: The diagrams reordered to be translations in lower index of each other. The diagrams are of the form $u^1_n u^2_{n+1} u^1_{n+2}$ (top) and $u^2_n u^1_{n+1} u^2_{n+2}$ (bottom)

$$\begin{aligned}\dot{E}^{\alpha}_{\wedge\vee} = \sum_n ik_n k^{\alpha}_n \Big(& c_1 u^{(1)}_{n-2} u^{(2)}_{n-1} u^{*(1)}_n + b_1 u^{(2)}_{n-1} u^{*(1)}_n u^{(2)}_{n+1} + a_1 u^{*(1)}_n u^{(2)}_{n+1} u^{(1)}_{n+2} \\ & + c_2 u^{(2)}_{n-2} u^{(1)}_{n-1} u^{*(2)}_n + b_2 u^{(1)}_{n-1} u^{*(2)}_n u^{(1)}_{n+1} + a_2 u^{*(2)}_n u^{(1)}_{n+1} u^{(2)}_{n+2} \\ & - c_1 u^{*(1)}_{n-2} u^{*(2)}_{n-1} u^{(1)}_n - b_1 u^{*(2)}_{n-1} u^{(1)}_n u^{*(2)}_{n+1} - a_1 u^{(1)}_n u^{*(2)}_{n+1} u^{*(1)}_{n+2} \\ & - c_2 u^{*(2)}_{n-2} u^{*(1)}_{n-1} u^{(2)}_n - b_2 u^{*(1)}_{n-1} u^{(2)}_n u^{*(1)}_{n+1} - a_2 u^{(2)}_n u^{*(1)}_{n+1} u^{*(2)}_{n+2} \Big)\end{aligned} \tag{20}$$

To form triad pairs we need to fix the complex-conjugations of the governing equation. By choosing

$$\begin{aligned} a_1 u^{(2)}_{n+1} u^{(1)}_{n+2} &\to a_1 u^{*(2)}_{n+1} u^{(1)}_{n+2} \\ b_1 u^{(2)}_{n-1} u^{(2)}_{n+1} &\to b_1 u^{*(2)}_{n-1} u^{(2)}_{n+1} \\ a_2 u^{(1)}_{n+1} u^{(2)}_{n+2} &\to a_2 u^{*(1)}_{n+1} u^{(2)}_{n+2} \\ b_2 u^{(1)}_{n-1} u^{(1)}_{n+1} &\to b_2 u^{*(1)}_{n-1} u^{(1)}_{n+1} \end{aligned} \tag{21}$$

we can write

$$\begin{aligned}\dot{E}^{\alpha}_{\wedge\vee} = \sum_n ik_n k^{\alpha}_n \Big(& c_1 u^{(1)}_{n-2} u^{(2)}_{n-1} u^{*(1)}_n + b_1 u^{*(2)}_{n-1} u^{*(1)}_n u^{(2)}_{n+1} + a_1 u^{*(1)}_n u^{*(2)}_{n+1} u^{(1)}_{n+2} \\ & + c_2 u^{(2)}_{n-2} u^{(1)}_{n-1} u^{*(2)}_n + b_2 u^{*(1)}_{n-1} u^{*(2)}_n u^{(1)}_{n+1} + a_2 u^{*(2)}_n u^{*(1)}_{n+1} u^{(2)}_{n+2} \\ & - c_1 u^{*(1)}_{n-2} u^{*(2)}_{n-1} u^{(1)}_n - b_1 u^{(2)}_{n-1} u^{(1)}_n u^{*(2)}_{n+1} - a_1 u^{(1)}_n u^{(2)}_{n+1} u^{*(1)}_{n+2} \\ & - c_2 u^{*(2)}_{n-2} u^{*(1)}_{n-1} u^{(2)}_n - b_2 u^{(1)}_{n-1} u^{(2)}_n u^{*(1)}_{n+1} - a_2 u^{(2)}_n u^{(1)}_{n+1} u^{*(2)}_{n+2} \Big)\end{aligned} \tag{22}$$

which we now can rewrite in terms of triplets of translated triad pairs

$$\begin{aligned}\dot{E}^{\alpha}_{\wedge\vee} = i\sum_{n}\Big(&[k_n k_n^{\alpha} a_1 + k_{n+1}k_{n+1}^{\alpha} b_2 - k_{n+2}k_{n+2}^{\alpha}c_1]u_n^{(1)}u_{n+1}^{(2)}u_{n+2}^{*(1)} + \\ &[k_n k_n^{\alpha} a_2 + k_{n+1}k_{n+1}^{\alpha} b_1 - k_{n+2}k_{n+2}^{\alpha}c_2]u_n^{(2)}u_{n+1}^{(1)}u_{n+2}^{*(2)} - c.c\Big)\end{aligned} \tag{23}$$

We choose the interactions from this diagram to be symmetric such that $a_1 = a_2 = a$, $b_1 = b_2 = b$ and $c_1 = c_2 = c$, this yields

$$i\sum_{n} k_n k_0^{\alpha}\lambda^{n(\alpha+1)}\left(a + b\lambda^{\alpha+1} - c\lambda^{2(\alpha+1)}\right)\left[u_n^{(1)}u_{n+1}^{(2)}u_{n+2}^{*(1)} + u_n^{(2)}u_{n+1}^{(1)}u_{n+2}^{*(2)} - c.c\right] \tag{24}$$

Now rescaling the coefficients as $\tilde{a} = a$, $\tilde{b} = b\lambda$, $\tilde{c} = c\lambda^2$ and letting $z = \lambda^{\alpha}$, we can write

$$i\sum_{n} k_n k_0^{\alpha}\lambda^{n(\alpha+1)}\left(\tilde{a} + \tilde{b}z - \tilde{c}z^2\right)\left[u_n^{(1)}u_{n+1}^{(2)}u_{n+2}^{*(1)} + u_n^{(2)}u_{n+1}^{(1)}u_{n+2}^{*(2)} - c.c\right] \tag{25}$$

Thus, if $\tilde{a} + \tilde{b}z - \tilde{c}z^2 = 0$, the sum is conserved within the diagrams. This is equivalent to $1 + bz + cz^2 = 0$ where we have simply divided through by $\tilde{a}$ and rescaled $b = \tilde{b}/\tilde{a}$ and $c = \tilde{c}/\tilde{a}$. Demanding that the energy ($\alpha = 0$) be conserved within the triad sets one of the solutions $z_1 = \lambda^0 = 1$, and provides that $1 + b - c = 0$. Following the notation of the Sabra model we write $b = -\epsilon_{\wedge\vee}$ and $c = 1 - \epsilon_{\wedge\vee}$, where we are free to choose the parameter $\epsilon_{\wedge\vee}$. This then provides the second solution

$$z = \frac{\epsilon_{\wedge\vee} \pm \sqrt{\epsilon_{\wedge\vee}^2 + 4(1-\epsilon_{\wedge\vee})}}{-2(1-\epsilon_{\wedge\vee})} = \frac{\epsilon_{\wedge\vee} \pm (\epsilon_{\wedge\vee} - 2)}{2(\epsilon_{\wedge\vee} - 1)} = \begin{cases} z_1 = 1 \\ z_2 = z_{\wedge\vee} = \frac{1}{\epsilon_{\wedge\vee} - 1} \end{cases} \tag{26}$$

which then provides the $\alpha_{\wedge\vee}$ for the second conserved sum within the diagram $\alpha_{\wedge\vee} = \frac{log(|z_{\wedge\vee}|) - i\pi}{log(\lambda)}$. The terms contributed to governing equations are therefore

$$\Gamma^{(1)}_{n,\wedge\vee} = u_{n+1}^{*(2)}u_{n+2}^{(1)} - \frac{\epsilon_{\wedge\vee}}{\lambda}u_{n-1}^{*(2)}u_{n+1}^{(2)} - \frac{\epsilon_{\wedge\vee} - 1}{\lambda^2}u_{n-1}^{(2)}u_{n-2}^{(1)} \tag{27}$$

$$\Gamma^{(2)}_{n,\wedge\vee} = u_{n+1}^{*(1)}u_{n+2}^{(2)} - \frac{\epsilon_{\wedge\vee}}{\lambda}u_{n-1}^{*(1)}u_{n+1}^{(1)} - \frac{\epsilon_{\wedge\vee} - 1}{\lambda^2}u_{n-1}^{(1)}u_{n-2}^{(2)} \tag{28}$$

Demanding the conservation of energy within the diagrams of Figure 8, 9 and 10 in *Appendix A* follows the same procedure, however we introduce the free parameters $\epsilon_{\Leftarrow}$, $\epsilon_{\Rightarrow}$ and $\epsilon_{\square}$ associated with the diagrams in that order, which relates to their respective z's and α's as above. The contributions from the remaining diagrams are found in *Appendix A*. We can now write the governing equations as

$$\dot{u}_n^{(i)} = ik_n\left(\Gamma^{(i)}_{n,Sabra} + \Gamma^{(i)}_{n,\wedge\vee} + \Gamma^{(i)}_{n,\Rightarrow} + \Gamma^{(i)}_{n,\Leftarrow} + \Gamma^{(i)}_{n,\square}\right) - \nu k_n^2 u_n^{(i)} - \nu k_n^{-2}u_n^{(i)} + f_n \tag{29}$$

where $\Gamma^{(i)}_{n,Sabra} = u_{n+1}^{*(i)}u_{n+1}^{(i)} - \frac{\epsilon_i}{\lambda}u_{n-1}^{*(i)}u_{n+1}^{(i)} - \frac{\epsilon_i - 1}{\lambda}u_{n-2}^{(i)}u_{n-1}^{(i)}$ with ϵ_i being the ϵ associated with the interactions in the chains. The term $-\nu k_n^{-2}$ has been added to simulate large scale friction, significant only at small wavenumbers. For each diagram there is a second inviscid invariant, and we can therefore construct at second inviscid invariant for the whole system by adding all the conserved terms with $\alpha \neq 0$ from each diagram type, as

$$\dot{E}^{\alpha_2} = \dot{E}^{\alpha_{Sabra}} + \dot{E}^{\alpha_{\wedge\vee}} + \dot{E}^{\alpha_{\Rightarrow}} + \dot{E}^{\alpha_{\Leftarrow}} + \dot{E}^{\alpha_{\square}} \tag{30}$$

However, constructing the inviscid invariant function E^{α_2} is not straight forward, since the inviscid invariants are only invariants when the α's are coupled to the correct diagrams. In other words, the function $E^{\alpha_{\vee\wedge}} = \sum_{n=1}^{N} k_n^{\alpha_{\vee\wedge}} \left(\left| u_n^{(1)} \right|^2 + \left| u_n^{(2)} \right|^2 \right)$ is not a conserved quantity, since then $\dot{E}^{\alpha_{\vee\wedge}}$ is a sum over all diagrams, but associated with $k^{\alpha_{\vee\wedge}}$. One could construct a function that picks the correct α's in $\dot{E}^{\alpha_2}$ given the diagrams Γ, however then E^{α_2} would be undefined as it would also be a function of the diagrams Γ which are ambiguous in E^{α_2}. It seems plausible that a second inviscid invariant for the whole systems exists, and its time-derivative can be written as in Equation 30, however defining such a function will be left for further investigations.

Regardless, in the limit where all ϵ's are equal, $E^{\alpha_2} = \sum_{n=1}^{N} k_n^{\alpha_2} \left(\left| u_n^{(1)} \right|^2 + \left| u_n^{(2)} \right|^2 \right)$ is indeed conserved, and is just the helcity/enstrophy. In this case the coupled model should act as the Sabra model, which is what one sees when comparing Figure 1 and 6.

4 Results

When integrating the coupled model the same shell spacing $\lambda = 2$, $k_0 = 1$, and number of shells $N = 20$ will be used throughout. We use a 5'th order Rosenbeck method for integrating the stiff system of ODE's, with a fixed timestepping.

By enforcing the energy conservation, we expect equipartition of energy, resulting in a flat spectrum, in the unforced and inviscid case. In Figure 5 the coupled model has been integrated from a random initial condition, multiplied with a Kolmogorov scaling $k^{-1/3}$, for a total time of $t = 2$ with timestepping $\Delta t = 5 \times 10^{-7}$. The large wavenumbers evolve towards a flat distribution, however since the total runtime is low, the small wavenumbers do not have time to evolve to equipartition since the eddies have a larger turn-over time. It is reasonable that the timestepping needs to be significantly smaller than in the follow simulations with dissipation, since the dissipative term kills most dynamics at large shell numbers. Since these are the smallest scales needed to be resolved in the stiff system, with fast dynamics, suppressing these shells considerably beyond Kolmogorov scale reduces the required time-resolution. To obtain better statistics one would need to lower Δt for a solution that is stable for longer integration times.

The coupled model is now integrated for different choices of ϵ's (see *Appendix B* for a table of configurations). For all simulations the initial condition is zero velocity with viscosity $\nu = 5 \times 10^{-7}$ and forcing $f_n = 0.1 \times (1 + i) \times (\delta_{n,7} + \delta_{n,8})$. The spectra of the velocities are shown in Figure 6 and 7, where simulations for the 3D limit (all ϵ's set to 1/2) and 2D limit (all ϵ's set to 5/4) are shown, to indicate how much the coupled models with mixed ϵ's compare to the 3D and 2D cases. The spectra in both limits have ranges where they follow the expected scaling behaviour of $|u| \sim k^{-1/3}$ for 3D and $|u| \sim k^{-1}$ for 2D. For most combinations of parameters (Mix 1, Mix 2, Mix 3), the spectra follow that of the 3D limit, following the scaling determined but the energy cascade for wavenumbers larger than where the forcing is applied. For lower shell numbers than where forcing is applied, these spectra are approximately flat as there is no cascade, which is the same behaviour seen for the Sabra model in Figure 1.

Only when a single interaction is 3D with an $\epsilon = 0.9$ (Mix 4), close to the singular transition at $\epsilon = 1$, does it resemble the 2D spectrum, with a range that has a k^{-1} scaling. There is a significant dip at shell number 1, which is either due to the large scale dissipation or poor statistics. For shell numbers lower than the forced shells there is a stark difference in the 2D and 3D behaviour, where Mix 4 is markedly more 2D like, however for the tail end of the spectra, for shell numbers large than the where the forcing is applied, there is a more gradual transitions from 3D to 2D behaviour.

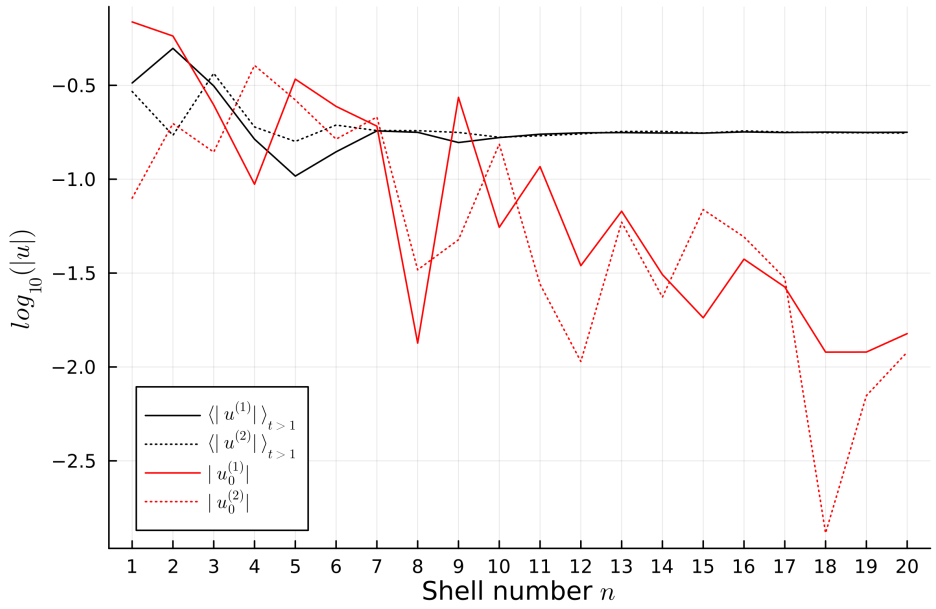

Figure 5: Simulation of the coupled model with random initial condition, and parameters $[\lambda, k_0, N, \Delta t] = \left[2, 1, 20, 1 \times 10^{-7}\right]$. The ϵ's used are $[\epsilon_1, \epsilon_2, \epsilon_{\vee\wedge}, \epsilon_{\Rightarrow}, \epsilon_{\Leftarrow}, \epsilon_{\square}] = [1/2, 5/4, 4/5, 4/5, 4/5, 4/5]$, running for a total time of $t = 2$. For longer run times and better statistics the timestepping needs to be lowered. The red lines are the initial condition, and the black the averages from times $t > 1$.

In Figure 7 the spectra of the $|u_n^{(2)}|$ shells, from the same simulations as in Figure 6, are shown. These greatly resemble the $|u_n^{(1)}|$ spectra, showing that the scaling behaviour throughout the model is consistent, in contrast to what one might expect when $\epsilon_1 = 1/2$ and $\epsilon_2 = 5/4$. The remaining interactions therefore play a big role in the behaviour of the model.

5 Discussion

From the simulations of different configurations, it seems that the 3D scaling is dominating in the coupled model, since 2D scaling is only seen when approaching the 2D limit (Mix 4). This behaviour is somewhat to be expected, due to the asymmetry of cascades in 3D and 2D for the Sabra model. The transport of enstrophy to larger shell numbers seems completely dominated by the scaling of the energy cascade for shell numbers larger than where forcing is applied, when not close to the 2D limit. However, that this behaviour be so pronounced indicates that there are likely non-linear effects that become dominant when approaching the the 2D limit. This calls for both a better parameter scan near the configuration of Mix 4, but also an analytical study of the non-linear fluxes in the coupled model, which could illuminate when the model expresses the two regimes. Such a study would include obtaining a well-defined expression for the second inviscid invariant.

For Mix 4 we do not expect equipartition for small shell numbers, yet the spectrum is flat. This is likely due to the dissipation at large scales killing the otherwise non-flat scaling. To determine if this is indeed the case, it would therefore be pertinent to do simulations where the large scale dissipation is either removed or lowered in strength,

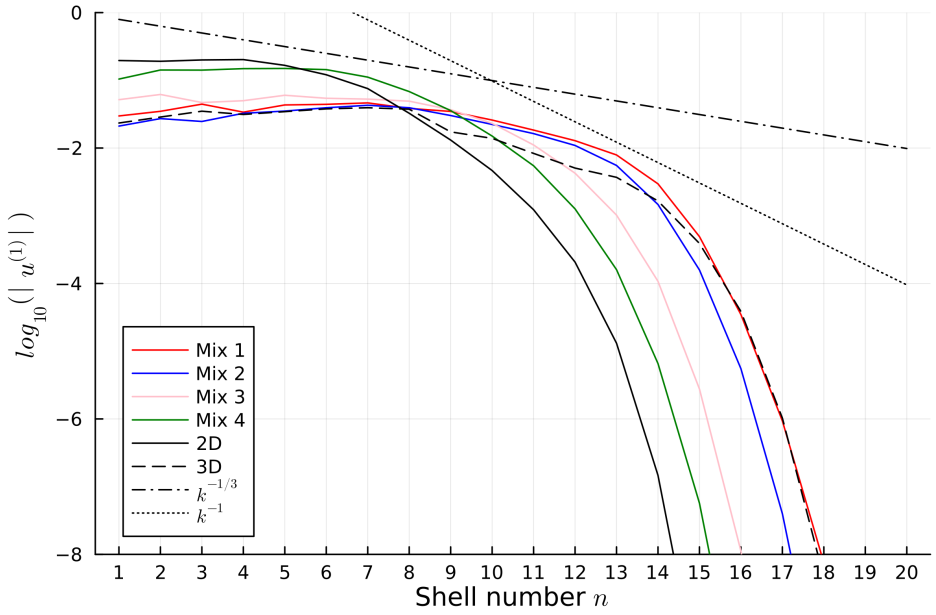

Figure 6: Spectra of $|u^(1)|$ of the coupled model for different configurations of ϵ's, all with forcing $f_n = 0.1 \times (1+i) \times (\delta_{n,7} + \delta_{n,8})$, and dissipation at both large and small scales. For all cases the parameters used are $[\lambda,\, k_0,\, N,\, \Delta t] = \left[2,\, 1,\, 20,\, 5 \times 10^{-5}\right]$ with a total time of $t = 120$, and averaging for times $t > 5$. The 3D and 2D spectra are for setups where all ϵ's are either 1/2 or 5/4. We highlight Mix 4 where $[\epsilon_1,\, \epsilon_2,\, \epsilon_{\vee\wedge},\, \epsilon_{\Rightarrow},\, \epsilon_{\Leftarrow},\, \epsilon_{\square}] = [0.9,\, 5/4,\, 5/4,\, 5/4,\, 5/4,\, 5/4]$ and Mix 1 for which $[\epsilon_1,\, \epsilon_2,\, \epsilon_{\vee\wedge},\, \epsilon_{\Rightarrow},\, \epsilon_{\Leftarrow},\, \epsilon_{\square}] = [1/2,\, 5/4,\, 1/2,\, 5/4,\, 5/4,\, 1/2]$. The remaining configurations can be found in *Appendix B*.

either by assigning another ν at this scale or changing the exponent in the k^{-2} term.

The scaling in Figures 6 and 7 are difficult to investigate since, due to the choice of parameters, the inertial ranges, where the relevant scaling behaviour is found, are not very big. By lowering the dissipation ν in the system, and increasing the number of shells simulated, the inertial range would be extended, making the determination of scaling properties more accessible.

The coupled model is made based on the assumption that the two Sabra models that are coupled have the same shell structure in Fourier-space. To make the model resemble the 2D scaling at low wavenumbers, with two distinct regimes of scaling before and after the forcing, it seems plausible that extending the 2D chain to include smaller wave numbers could aid this process. The extended shells would then be dominated by the 2D interactions, as long as the number of shells which the 2D chain is extended with exceeds 3, and an inverse transport of energy might be obtained. Of course this could also be done for the 3D chain, extending at larger shell numbers, but here the 3D effects already dominate.

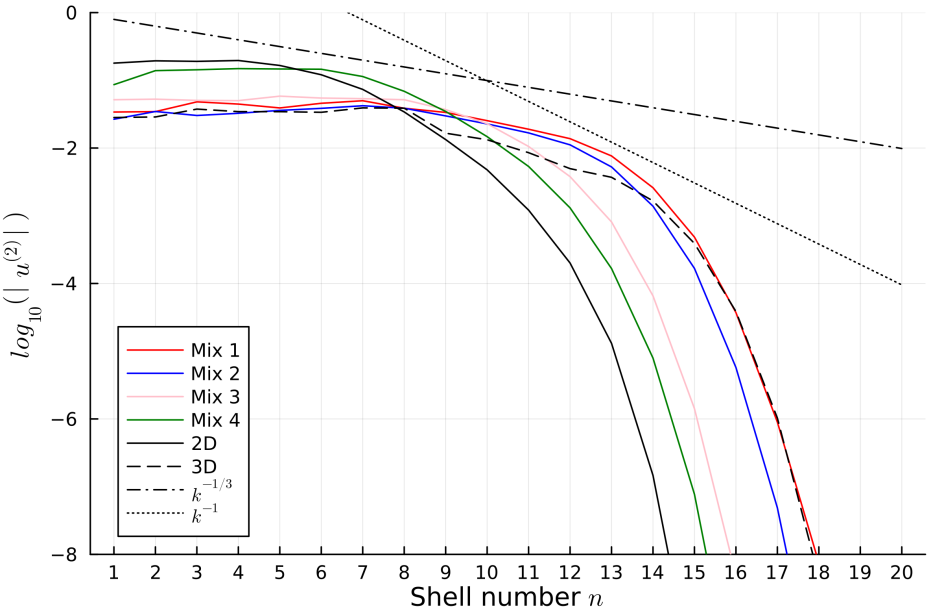

Figure 7: Spectra of $|u_n^{(2)}|$ for the same configurations and parameters as in Figure 6.

6 Conclusion

In this project, a coupled shell model of turbulence has been proposed, to capture the inherent 2D and 3D spectral scaling of velocities in atmospheric turbulence. For the parameter space explored in this project, the 3D effects in the coupled model dominate the scaling properties. This property seems to an affect of the presence of an energy cascade in the 3D Sabra model, and a missing inverse cascade in 2D. To determine if this is indeed the case, further investigation is required both in further scanning of the parameter space, and analytical work on the coupled model.

References

[1] Peter D. Ditlevsen. Symmetries, invariants, and cascades in a shell model of turbulence. *Physical Review E*, 62(1):484, 2000.

[2] Peter D. Ditlevsen. *Turbulence and Shell Models*. Cambridge University Press, November 2010.

[3] A. N. Kolmogorov. The local structure of turbulence in incompressible viscous fluid for very large reynolds numbers. *Proceedings: Mathematical and Physical Sciences*, 434(1890):9–13, 1991.

[4] C. E. Leith. Atmospheric predictability and two-dimensional turbulence. *Journal of Atmospheric Sciences*, 28(2):145–161, 1971.

[5] G. D. Nastrom and K. S. Gage. A climatology of atmospheric wavenumber spectra of wind and temperature observed by commercial aircraft. *Journal of Atmospheric Sciences*, 42(9):950–960, 1985.

7 Appendix A: Diagrams

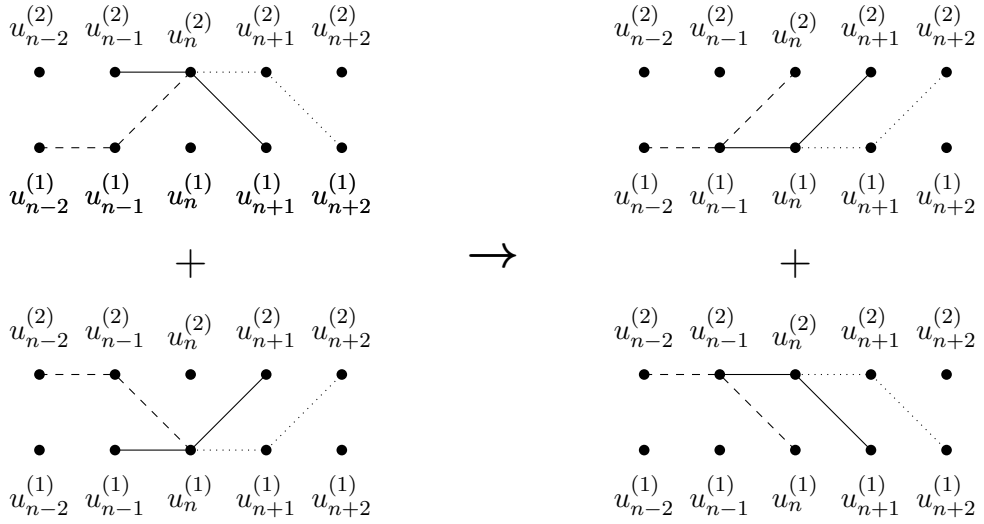

Figure 8: The possible triad interactions of the form $u^i_n u^i_{n+1} u^j_{n+2}$. On the r.h.s the form $u^1_n u^1_{n+1} u^2_{n+2}$ (top) and $u^2_n u^2_{n+1} u^1_{n+2}$ (bottom)

The energy change associated with Figure 8 is

$$\begin{aligned}\dot{E}^{\alpha}_{\Rightarrow} = \sum_n ik_n k_n^{\alpha}\Big(&c_1 u^{(2)}_{n-2}u^{(2)}_{n-1}u^{*(1)}_{n} + b_1 u^{(1)}_{n-1}u^{*(1)}_{n}u^{(2)}_{n+1} + a_1 u^{*(1)}_{n}u^{(1)}_{n+1}u^{(2)}_{n+2}\\ &+ c_2 u^{(1)}_{n-2}u^{(1)}_{n-1}u^{*(2)}_{n} + b_2 u^{(2)}_{n-1}u^{*(2)}_{n}u^{(1)}_{n+1} + a_2 u^{*(2)}_{n}u^{(2)}_{n+1}u^{(1)}_{n+2}\\ &- c_1 u^{*(2)}_{n-2}u^{*(2)}_{n-1}u^{(1)}_{n} - b_1 u^{*(1)}_{n-1}u^{(1)}_{n}u^{*(2)}_{n+1} - a_1 u^{(1)}_{n}u^{*(1)}_{n+1}u^{*(2)}_{n+2}\\ &- c_2 u^{*(1)}_{n-2}u^{*(1)}_{n-1}u^{(2)}_{n} - b_2 u^{*(2)}_{n-1}u^{(2)}_{n}u^{*(1)}_{n+1} - a_2 u^{(2)}_{n}u^{*(2)}_{n+1}u^{*(1)}_{n+2}\Big)\end{aligned} \tag{31}$$

fixing the complex conjugations such that

$$\begin{aligned}a_1 u^{(1)}_{n+1}u^{(2)}_{n+2} &\to a_1 u^{*(1)}_{n+1}u^{(2)}_{n+2}\\ b_1 u^{(1)}_{n-1}u^{(2)}_{n+1} &\to b_1 u^{*(1)}_{n-1}u^{(2)}_{n+1}\\ a_2 u^{(2)}_{n+1}u^{(1)}_{n+2} &\to a_2 u^{*(2)}_{n+1}u^{(1)}_{n+2}\\ b_2 u^{(2)}_{n-1}u^{(1)}_{n+1} &\to b_2 u^{*(2)}_{n-1}u^{(1)}_{n+1}\end{aligned} \tag{32}$$

The energy change can be written as

$$\dot{E}^{\alpha}_{\Rightarrow} = i\sum_n k_n k_0^{\alpha}\lambda^{n(\alpha+1)}\left(\tilde{a}+\tilde{b}z-\tilde{c}z^2\right)\left[u^{(2)}_{n}u^{(2)}_{n+1}u^{*(1)}_{n+2} + u^{(1)}_{n}u^{(1)}_{n+1}u^{*(2)}_{n+2} - c.c\right] \tag{33}$$

and the additional terms become

$$\Gamma^{(1)}_{n,\Rightarrow} = u^{*(1)}_{n+1}u^{(2)}_{n+2} - \frac{\epsilon_{\Rightarrow}}{\lambda}u^{*(1)}_{n-1}u^{(2)}_{n+1} - \frac{\epsilon_{\Rightarrow}-1}{\lambda^2}u^{(2)}_{n-1}u^{(2)}_{n-2} \tag{34}$$

$$\Gamma^{(2)}_{n,\Rightarrow} = u^{*(2)}_{n+1}u^{(1)}_{n+2} - \frac{\epsilon_{\Rightarrow}}{\lambda}u^{*(2)}_{n-1}u^{(1)}_{n+1} - \frac{\epsilon_{\Rightarrow}-1}{\lambda^2}u^{(1)}_{n-1}u^{(1)}_{n-2} \tag{35}$$

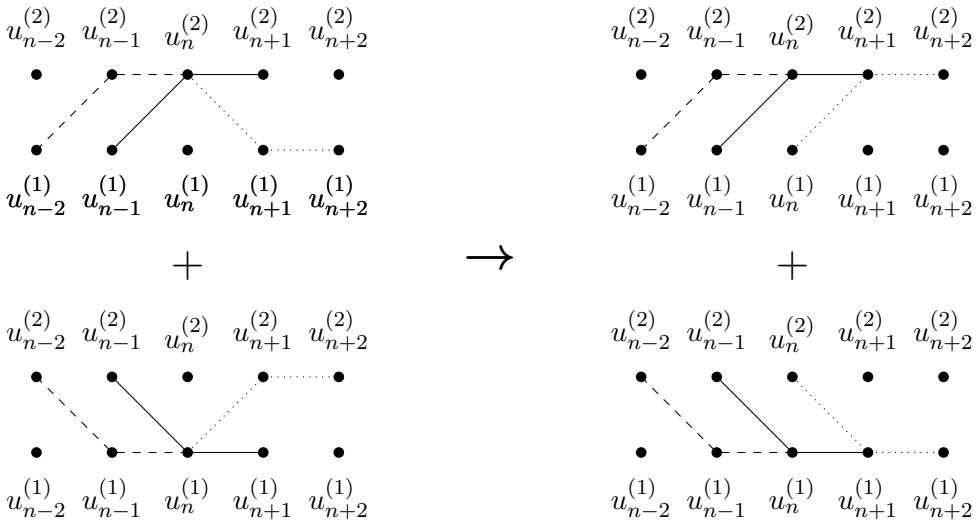

Figure 9: The possible triad interactions of the form $u^i_n u^j_{n+1} u^j_{n+2}$. On the r.h.s the form $u^1_n u^2_{n+1} u^2_{n+2}$ (top) and $u^2_n u^1_{n+1} u^1_{n+2}$ (bottom)

We do exactly the same for the diagrams in Figure 9, where we have that

$$\begin{aligned}\dot{E}^{\alpha}_{\Leftarrow} = \sum_n ik_n k^{\alpha}_n \Big(& c_1 u^{(2)}_{n-2}u^{(1)}_{n-1}u^{*(1)}_n + b_1 u^{(2)}_{n-1}u^{*(1)}_n u^{(1)}_{n+1} + a_1 u^{*(1)}_n u^{(2)}_{n+1}u^{(2)}_{n+2} \\ & + c_2 u^{(1)}_{n-2}u^{(2)}_{n-1}u^{*(2)}_n + b_2 u^{(1)}_{n-1}u^{*(2)}_n u^{(2)}_{n+1} + a_2 u^{*(2)}_n u^{(1)}_{n+1}u^{(1)}_{n+2} \\ & - c_1 u^{*(2)}_{n-2}u^{*(1)}_{n-1}u^{(1)}_n - b_1 u^{*(2)}_{n-1}u^{(1)}_n u^{*(1)}_{n+1} - a_1 u^{(1)}_n u^{*(2)}_{n+1}u^{*(2)}_{n+2} \\ & - c_2 u^{*(1)}_{n-2}u^{*(2)}_{n-1}u^{(2)}_n - b_2 u^{*(1)}_{n-1}u^{(2)}_n u^{*(2)}_{n+1} - a_2 u^{(2)}_n u^{*(1)}_{n+1}u^{*(1)}_{n+2} \Big)\end{aligned} \tag{36}$$

and again performing the complex conjugations as follows

$$\begin{aligned} a_1 u^{(2)}_{n+1}u^{(2)}_{n+2} &\to a_1 u^{*(2)}_{n+1}u^{(2)}_{n+2} \\ b_1 u^{(1)}_{n-1}u^{(1)}_{n+1} &\to b_1 u^{*(1)}_{n-1}u^{(1)}_{n+1} \\ a_2 u^{(1)}_{n+1}u^{(1)}_{n+2} &\to a_2 u^{*(1)}_{n+1}u^{(1)}_{n+2} \\ b_2 u^{(2)}_{n-1}u^{(2)}_{n+1} &\to b_2 u^{*(2)}_{n-1}u^{(2)}_{n+1} \end{aligned} \tag{37}$$

now seeing that we can write

$$\dot{E}^{\alpha}_{\Leftarrow} = i\sum_n k_n k^{\alpha}_0 \lambda^{n(\alpha+1)} \left(\tilde{a} + \tilde{b}z - \tilde{c}z^2\right) \left[u^{(2)}_n u^{(1)}_{n+1}u^{*(1)}_{n+2} + u^{(1)}_n u^{(2)}_{n+1}u^{*(2)}_{n+2} - c.c\right] \tag{38}$$

providing the non-linear terms

$$\Gamma^{(1)}_{n,\Leftarrow} = u^{*(2)}_{n+1}u^{(2)}_{n+2} - \frac{\epsilon_{\Leftarrow}}{\lambda}u^{*(2)}_{n-1}u^{(1)}_{n+1} - \frac{\epsilon_{\Leftarrow}-1}{\lambda^2}u^{(1)}_{n-1}u^{(2)}_{n-2} \tag{39}$$

$$\Gamma^{(2)}_{n,\Leftarrow} = u^{*(1)}_{n+1}u^{(1)}_{n+2} - \frac{\epsilon_{\Leftarrow}}{\lambda}u^{*(1)}_{n-1}u^{(2)}_{n+1} - \frac{\epsilon_{\Leftarrow}-1}{\lambda^2}u^{(2)}_{n-1}u^{(1)}_{n-2} \tag{40}$$

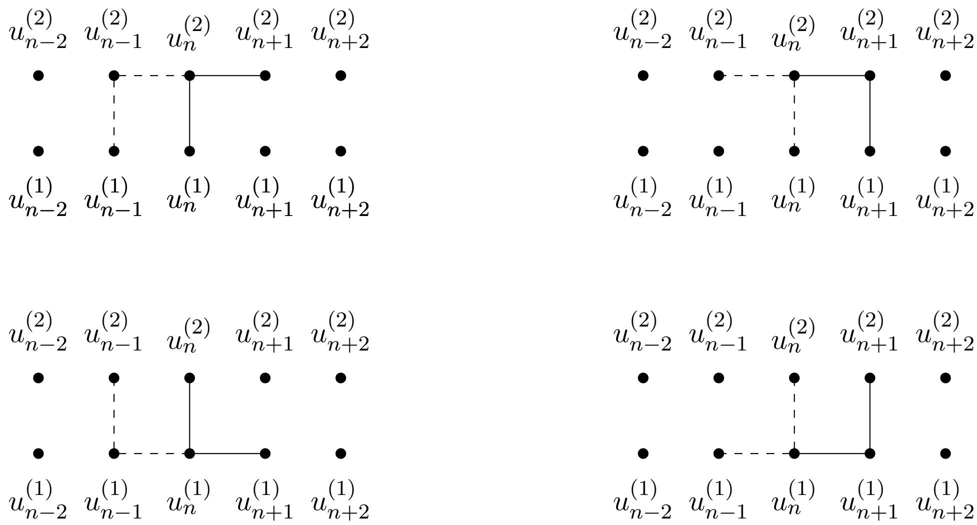

Figure 10: In clockwise fashion, starting from the top right: The possible triad interactions of the form $u^1_n u^2_n u^2_{n+1}$, $u^2_n u^2_{n+1} u^1_{n+1}$,$u^1_n u^1_{n+1} u^2_{n+1}$ and $u^2_n u^1_n u^1_{n+1}$.

To see that some diagrams in Figure 10 show up twice, we write out all terms in $u^{*(1)}_n \dot{u}^{(1)}_n$ and $u^{*(2)}_n \dot{u}^{(2)}_n$ containing such diagrams. Starting from the upper left diagrams

$$\begin{aligned} u^{*(1)}_n \dot{u}^{(1)}_{n,\ulcorner} + u^{*(2)}_n \dot{u}^{(2)}_{n,\ulcorner} + c.c =& ik_n \Big(a_1 u^{*(1)}_n u^{(2)}_n u^{(2)}_{n+1} + a_2 u^{(1)}_n u^{*(2)}_n u^{(2)}_{n+1} + a_3 u^{(1)}_{n-1} u^{(2)}_{n-1} u^{*(2)}_n \\ & -a_1 u^{(1)}_n u^{*(2)}_n u^{*(2)}_{n+1} - a_2 u^{*(1)}_n u^{(2)}_n u^{*(2)}_{n+1} - a_3 u^{*(1)}_{n-1} u^{*(2)}_{n-1} u^{(2)}_n \Big) \end{aligned} \tag{41}$$

letting $a_1 u^{(2)}_n u^{(2)}_{n+1} \to a_1 u^{(2)}_n u^{*(2)}_{n+1}$ and $a_3 u^{(1)}_{n-1} u^{(2)}_{n-1} \to a_3 u^{*(1)}_{n-1} u^{(2)}_{n-1}$gives

$$\begin{aligned} u^{*(1)}_n \dot{u}^{(1)}_{n,\ulcorner} + u^{*(2)}_n \dot{u}^{(2)}_{n,\ulcorner} + c.c =& ik_n \Big(a_1 u^{*(1)}_n u^{(2)}_n u^{*(2)}_{n+1} + a_2 u^{(1)}_n u^{*(2)}_n u^{(2)}_{n+1} + a_3 u^{*(1)}_{n-1} u^{(2)}_{n-1} u^{*(2)}_n \\ & -a_1 u^{(1)}_n u^{*(2)}_n u^{(2)}_{n+1} - a_2 u^{*(1)}_n u^{(2)}_n u^{*(2)}_{n+1} - a_3 u^{(1)}_{n-1} u^{*(2)}_{n-1} u^{(2)}_n \Big) \end{aligned} \tag{42}$$

thus the change in conserved integral associated with the diagram can be expressed as

$$\dot{E}^{\alpha}_{n,\ulcorner} = i\sum_n k_n k_0^{\alpha} \lambda^{n(\alpha+1)} \left(\tilde{a}_1 - \tilde{a}_2 + \tilde{b}z\right)\left[a_1 u^{*(1)}_n u^{(2)}_n u^{*(2)}_{n+1} - c.c\right] \tag{43}$$

where we let $\tilde{a}_i = a_i$ and $\tilde{b} = a_3\lambda$. If we assume that $\tilde{a}_1 = \tilde{a}_2 = \tilde{a}$, since they carry the interactions strengt of the same triad, the requirement that $\tilde{b}z = 0 \Rightarrow \tilde{b} = 0$ then follows. Therefore $\tilde{a}$ is a free parameter and to follow the convention of the choice of such parameters we let $\tilde{a} = \epsilon_{\ulcorner}$ and the contribution to the governing equations become

$$\Gamma^{(2)}_{n,\ulcorner} = \epsilon_{\ulcorner} u^{(1)}_n u^{(2)}_{n+1} \tag{44}$$

$$\Gamma^{(1)}_{n,\ulcorner} = \epsilon_{\ulcorner} u^{(2)}_n u^{*(2)}_{n+1} \tag{45}$$

For the upper right diagram we have

$$u^{*(1)}_n \dot{u}^{(1)}_{n,\urcorner} + u^{*(2)}_n \dot{u}^{(2)}_{n,\urcorner} + c.c = ik_n \Big(a_1 u^{*(1)}_n u^{(2)}_n u^{(2)}_{n-1} + a_2 u^{(1)}_n u^{*(2)}_n u^{(2)}_{n-1} + a_3 u^{(1)}_{n+1} u^{(2)}_{n+1} u^{*(2)}_n \\ - a_1 u^{(1)}_n u^{*(2)}_n u^{*(2)}_{n-1} - a_2 u^{*(1)}_n u^{(2)}_n u^{*(2)}_{n-1} - a_3 u^{*(1)}_{n+1} u^{*(2)}_{n+1} u^{(2)}_n \Big) \tag{46}$$

requiring the complex conjugations $a_1 u^{(2)}_n u^{(2)}_{n-1} \to a_1 u^{(2)}_n u^{*(2)}_{n-1}$ and $a_3 u^{(1)}_{n+1} u^{(2)}_{n+1} \to a_3 u^{*(1)}_{n+1} u^{(2)}_{n+1}$. The energy change can then be written as

$$\dot{E}^{\alpha}_{n,\urcorner} = i \sum_n k_n k_0^{\alpha} \lambda^{n(\alpha+1)} \left(\tilde{a}_1 - \tilde{a}_2 + \tilde{b} z \right) \left[a_1 u^{*(2)}_n u^{(1)}_{n+1} u^{*(2)}_{n+1} - c.c \right] \tag{47}$$

where now $\tilde{a}_i = a_i \lambda$ and $\tilde{b} = a_3$, and the condition that $\tilde{a}_1 = \tilde{a}_2 = \tilde{a}$ again dictates that $\tilde{b} = 0$. Again, letting $\tilde{a}_i = \epsilon_{\urcorner}$, the terms obtained in the governing equations are therefore

$$\Gamma^{(2)}_{n,\urcorner} = \frac{\epsilon_{\urcorner}}{\lambda} u^{(1)}_n u^{(2)}_{n-1} \tag{48}$$

$$\Gamma^{(1)}_{n,\urcorner} = \frac{\epsilon_{\urcorner}}{\lambda} u^{(2)}_n u^{*(2)}_{n-1} \tag{49}$$

The two bottom diagrams in Figure 10 are the symmetric counterparts in the upper index of the the top diagrams, and so the contributions are simply the same with changed upper index ($1 \leftrightarrow 2$)

$$\Gamma^{(1)}_{n,\llcorner} = \epsilon_{\llcorner} u^{(2)}_n u^{(1)}_{n+1} \tag{50}$$

$$\Gamma^{(2)}_{n,\llcorner} = \epsilon_{\llcorner} u^{(1)}_n u^{*(1)}_{n+1} \tag{51}$$

and

$$\Gamma^{(1)}_{n,\lrcorner} = \frac{\epsilon_{\lrcorner}}{\lambda} u^{(2)}_n u^{(1)}_{n-1} \tag{52}$$

$$\Gamma^{(2)}_{n,\lrcorner} = \frac{\epsilon_{\lrcorner}}{\lambda} u^{(1)}_n u^{*(1)}_{n-1} \tag{53}$$

For the ease of notation we collect all the terms as

$$\Gamma^{(i)}_{n,\square} = \Gamma^{(i)}_{n,\ulcorner} + \Gamma^{(i)}_{n,\llcorner} + \Gamma^{(i)}_{n,\urcorner} + \Gamma^{(i)}_{n,\lrcorner} \tag{54}$$

When simulating the coupled model, we will assume that $\epsilon_{\ulcorner} = \epsilon_{\urcorner} = \epsilon_{\llcorner} = \epsilon_{\lrcorner} = \epsilon_{\square}$.

8 Appendix B: Parameters

The combinations of ϵ's used for simulating the coupled models are given as in Table 8.

Name	$[\epsilon_1, \epsilon_2, \epsilon_{\vee\wedge}, \epsilon_{\Rightarrow}, \epsilon_{\Leftarrow}, \epsilon_{\square}]$
Mix 1	[1/2, 5/4, 1/2, 5/4, 5/4, 1/2]
Mix 2	[1/2, 5/4, 1/2, 5/4, 5/4, 5/4]
Mix 3	[0.5, 5/4, 5/4, 5/4, 5/4, 5/4]
Mix 4	[0.9, 5/4, 5/4, 5/4, 5/4, 5/4]

Table 1: Combinations of ϵ's used for simulations in Figure 6 and 7